JOURNAL OF AIRCRAFT
Vol. 42, No. 4, July–August 2005

Aeroelastic Stability Enhancement and Vibration Suppression in a Composite Helicopter Rotor

Senthil Murugan* and Ranjan Ganguli†
Indian Institute of Science, Bangalore 560 012, India

An optimization procedure to 1) reduce the 4/revolution oscillatory hub loads and 2) increase the lag mode damping of a four-bladed soft-in-plane hingeless helicopter rotor is developed using a two-level approach. At the upper level, response surface approximations to the objective function and constraints are used to find the optimal blade mass and stiffness properties for vibration minimization and stability enhancement. An aeroelastic analysis based on finite elements in space and time is used. The numerical sampling needed to obtain the response surfaces is done using the central composite design of the theory of design of experiments. The approximate optimization problem expressed in terms of quadratic response surfaces is solved using a gradient-based method. Optimization results for the vibration problem in forward flight with unsteady aerodynamic modeling show a vibration reduction of about 15%. The dominant loads are the vertical hub shear and the rolling and pitching moments, which are reduced by 22–26%. The results of stability enhancement problem show an increase of 6–125% in the lag mode damping. At the lower level, a composite box beam is designed to match the upper-level beam blade stiffness and mass using a genetic algorithm which permits the use of discrete ply angle design variables such as 0, ±45, and 90 deg, which are easier to manufacture. Three different composite materials are used for designing the composite box beam, thus, showing the robustness of the genetic algorithm approach. Boron/epoxy composite gives the most compact box beam, whereas graphite/epoxy gives the lightest box beam.

Nomenclature

a	=	lift curve slope
b	=	composite box beam outer breadth
$\boldsymbol{C}$	=	finite element damping matrix
C_T	=	rotor thrust coefficient
c_b	=	blade chord
EA, EI_y, EI_z	=	blade axial, flap, and lag stiffness
$\boldsymbol{F}$	=	finite element force vector
F_x^{np}, F_y^{np}, F_z^{np}	=	n/revolution longitudinal, lateral, and vertical forces in the fixed frame
$f(\boldsymbol{X})$	=	objective function
GJ	=	blade torsional stiffness
$g_j(\boldsymbol{X})$	=	inequality constraint
h	=	composite box beam outer height
I_b	=	blade mass moment of inertia
J_{dn}^i	=	scalar norm of n/revolution blade root loads
J_v, J_s, J	=	objective function for vibration reduction, stability enhancement, and composite box-beam design
$\boldsymbol{K}$	=	finite element stiffness matrix
$\boldsymbol{M}$	=	finite element mass matrix
M_x, M_y, M_z	=	resultant blade bending moments in x, y, and z directions
M_x^{np}, M_y^{np}, M_z^{np}	=	n/revolution rolling, pitching, and yawing moments in the fixed frame
m	=	blade section mass
m_0	=	reference mass per unit length of blade
$\boldsymbol{p}$	=	modal displacement vector
Q_x	=	blade axial force
R	=	rotor radius
u_e	=	axial deformation of blade
v_b	=	lag deformation of blade
w_b	=	flap deformation of blade
$\boldsymbol{X}$	=	vector of design variables
x_i	=	coded design variable
α_k	=	decay rate of the kth mode
β_0, β_i, β_{ij}	=	regression coefficients of the response surface model
γ	=	lock number
ζ	=	percent damping of the lag mode
Θ	=	trim controls
θ	=	ply angle orientation
λ_k	=	eigenvalue of the kth mode
μ	=	rotor advance ratio
ν	=	Poisson's ratio
ρ	=	density of the air
σ	=	rotor solidity ratio
ϕ	=	elastic twist
Ω	=	rotation speed, scalar quantity
ω_k	=	Floquet stability frequency of the kth mode

Received 9 October 2003; revision received 10 September 2004; accepted for publication 5 October 2004.

*Graduate Student, Department of Aerospace Engineering; murga@aero.iisc.ernet.in.

†Assistant Professor, Department of Aerospace Engineering; ganguli@aero.iisc.ernet.in. Senior Member AIAA.

Introduction

THE main rotor is the crucial subsystem in a helicopter and provides lift, propulsive force, and control capability. Therefore, the design of the main rotor is an important problem that has received considerable attention. Rotor blades are slender flexible beams, which can undergo elastic deformations in bending and torsion that can be beyond the limits of linear beam theories. Furthermore, the deflections of the blade interact with the aerodynamic loading, which in turn is coupled with the structural dynamics because much of the elastic deformation and damping in flap and lag bending and in torsion is of aerodynamic origin. Therefore, the prediction of helicopter blade and hub loads and aeroelastic stability is an integrated nonlinear aeroelastic problem. The suppression of helicopter vibration and enhancement of aeroelastic stability is a key goal of research.[1] Although approaches based on active control are undergoing considerable research,[2] they suffer from cost and reliability problems. An alternative approach is to use optimization

methods to develop a low-vibration rotor and to enhance aeroelastic stability.

In recent years, considerable research has been directed toward the application of aeroelastic optimization methodology to improve the helicopter performance. Ganguli and Chopra[3] and Yaun and Friedmann[4] carried out optimization studies for rotor blades with swept tips and for composite rotors. Other recent studies in helicopter rotor optimization includes those by McCarthy and Chattopadhyay for tilt rotors,[5] Heverly et al. for optimal actuator placement,[6] Kim and Sarigul-Klijn for articulated rotors,[7] Soykasap and Hodges for composite tilt rotors,[8] Hathaway and Gandhi for aeromechanical stability,[9] and Celi[10] and Spence and Celi[11] for maneuver flight. A recent survey on helicopter optimization studies is provided by Ganguli.[12] Very few works have been done to maximize the damping of the rotor lag mode using aeroelastic optimization.[9,13] Fusato and Celi[13] present a design optimization study in which the damping of the rotor lag mode is maximized with constraints on rotor stability, loads, and handling qualities. In their work, lag mode damping is increased by 90% while satisfying all of the constraints, primarily by reducing the blade torsion stiffness.

The helicopter rotor dynamics analysis involves complex computer analyses, which are computationally expensive to perform. These analyses involve the solution of a nonlinear rotor dynamics equation to obtain the helicopter trim condition and aeroelastic stability condition. In the conventional aeroelastic optimization studies, the large aeroelastic analysis program has to be integrated with the optimization software, which can make the problem cumbersome. Gradient-based approaches to optimization require that the sensitivity derivatives either be calculated analytically or by finite difference. Finite difference derivatives are computationally expensive to calculate, and the selection of an appropriate step size can be difficult. Analytical and semi-analytical derivatives have been used by Spence and Celi,[11] Lu and Murthy,[14] Lim and Chopra,[15] and Ganguli and Chopra.[3,16] These derivatives are obtained using chain rule differentiation and are included in the computer program for aeroelastic analysis as an integral part. Analytical derivatives are more accurate than finite differences, and large savings of computer time are possible. However, analytical derivatives are difficult to implement in an industry setting.

One approach to overcome this difficulty is to use statistical techniques to construct approximations of the analyses,[17] instead of integrating the computer programs. Response surface (RS) methodology is one such statistical method used to construct approximations.[18] RSs for objective and constraint functions are created by sampled numerical experiments over the design space.[19] The RS models created then replace the computationally expensive analyses and facilitate fast analysis and exploration of the design space. Low-order polynomials are mostly used as the RS approximating functions.

In helicopter aeroelastic optimization, very limited work has been done using RS methodology. Henderson et al.[20] have applied RS techniques to helicopter rotor blade optimization using a two-level approach. The upper-level objective function was a linear combination of performance and dynamic measures. Upper-level design variables include pretwist, blade stiffnesses, tuning masses, and tuning locations. The lower level optimization assures that a structure can be sized to provide the stiffnesses required by the upper level and assures the structural integrity of the blade. However, in this study,[20] RS approximations were used for the cross-section design problem and not as an approximation to the rotor aeroelastic analysis.

Neural networks can also be used as the approximation to the rotor aeroelastic analysis. Lee and Hajela[21] approximated the objective function and constraints with neural surrogate functions. The neural networks, although good universal function approximations, have a black-box nature and are difficult to use in an industry setting. In contrast, polynomial RSs are easy to understand and capture the key slopes and curvatures of the design space while smoothing out local changes, which avoids the problem of spurious local minima. The problem solved in Ref. 21 was computationally intensive, and parallel computing was used.

Ganguli[22] showed that second-order polynomial RS could be used as an approximation for the aeroelastic analysis in helicopter rotor design optimization. In this study, unconstrained minimization of the 4/revolution hub loads was considered with flap, lag, and torsional stiffness as design variables. However, in this study, quasi-steady aerodynamics was used to calculate the vibratory hub loads and no restrictions on dynamic stresses were imposed. Furthermore, the enhancement of aeroelastic stability and the design of the composite rotor blade cross section for the optimal values was not addressed.

Many of the optimization studies end up with the optimal sectional properties for a one-dimensional beam blade used in rotor aeroelastic analysis and do not address the design of the actual two dimensional blade cross section. To have the complete box-beam design at the end of optimization, one approach is to perform the optimization using one-dimensional blade cross-sectional properties as design variables (upper-level problem) and then to design the two-dimensional cross section to match the optimal one-dimensional cross-sectional properties (lower-level problem). The helicopter rotor blades usually consists of a composite box-beam blade spar as the primary load carrying component. Therefore, two-dimensional section design variables are usually box-beam dimensions such as width, height, and wall thickness and ply angles of laminated walls. Soykasap[23] addressed this issue using the "inverse method" in tilt rotor optimization, in which the box beam is designed for the stiffness values obtained from the upper-level optimization problem. However, he used continuous ply angle design variables, which can be difficult to manufacture. In general, practical composite structures use discrete ply angles such as 0, ± 45, and 90 deg.

More frequently, the problem of composite blade cross-sectional design for given stiffness values has been formulated as a continuous design problem and solved using gradient-based optimization techniques.[23,24] These methods are not always successful for two reasons. First, the continuous values of design variables, such as ply angle orientation, must be rounded to the near integer value, which results in infeasible or suboptimal solutions. Second, there is noisy objective function and the existence of local extrema in the design space. In recent years, to overcome these problems, genetic algorithms (GA) have been successfully applied to composite structure optimization.[25] GAs are stochastic search techniques based on the mechanism of natural selection and natural genetics. The usual form of GA is described by Goldberg.[26] GAs are excellent all-purpose discrete algorithms, which can handle linear and nonlinear optimization problems or noisy search spaces by using payoff information (objective function) only. GAs are less likely than conventional optimization methods to get trapped in locally optimal areas of the search space. However, they are computationally expensive and are suitable for problems where the underlying analysis takes less computer time.

The objective of this study is to perform an aeroelastic optimization of a helicopter rotor for 1) minimizing vibration and 2) increasing the isolated rotor aeroelastic stability. RS approximations to the rotor aeroelastic analysis are used in the upper-level problem. The helicopter aeroelastic analysis is based on a finite element method in space and time. An unsteady aerodynamic model including impulsive and attached flow aerodynamics is used to calculate airloads. The vibration objective function includes all six components of 4/revolution hub loads for a four-bladed hingeless rotors and maintaining the constraints on dynamic stresses developed at the blade root, which are caused primarily by the 1/revolution and 2/revolution rotating frame vibratory loads. For the stability enhancement problem, the objective function is the percent damping of the least damped lag mode of the isolated rotor while the constraints are placed on blade vibration and dynamic stresses. The upper-level RS approximated optimization problem is solved using standard gradient-based algorithms. The lower-level problem of composite box-beam design for the section properties obtained from the upper-level optimization is solved using GA. The ability of GAs to handle discrete design variables is used for obtaining ply layups such as [0/$\pm$45/90 deg], which are easier to manufacture.

Helicopter Rotor Dynamic Analysis

In this work, a comprehensive aeroelastic analysis code, based on the finite element method, is used to evaluate the helicopter vibration and stability. The rotorcraft structure is modeled as a nonlinear representation of elastic rotor blades coupled to a rigid fuselage. The blade is modeled as a slender elastic beam undergoing flap bending, lag bending, elastic twist, and axial deflection. The effect of moderate deflections is included by retaining second-order nonlinear terms.[27] The blade is discretized into beam finite elements, each with 15 degrees of freedom. The finite element equations are reduced in size by using normal mode transformation. This results in the nonlinear ordinary differential equation with periodic coefficients,

$$\boldsymbol{M}\ddot{\boldsymbol{p}} + \boldsymbol{C}\dot{\boldsymbol{p}} + \boldsymbol{K}\boldsymbol{p} = \boldsymbol{F}(\boldsymbol{p}, \dot{\boldsymbol{p}}) \tag{1}$$

These equations are then solved using finite element in time in combination with the Newton–Raphson method. Equations (1) govern the dynamics of the rotor blade. The solutions to the equations are then used to calculate rotor blade loads using the force summation method, where aerodynamic forces are added to the inertial forces. The blade loads are integrated over the blade length and transformed to the fixed frame to obtain hub loads. The steady hub loads are used to obtain the forces acting on the rotor and combined with fuselage and tail rotor forces to obtain the helicopter rotor trim equations,

$$\boldsymbol{F}(\Theta) = \boldsymbol{0} \tag{2}$$

These nonlinear trim equations are also solved using the Newton–Raphson method. The helicopter rotor trim equations and the blade response equations in Eqs. (1) and (2) are solved simultaneously to obtain the blade steady response and hub loads. This coupled trim procedure is important for capturing the aeroelastic interaction between the aerodynamic forces and the blade deformations.

The rotorcraft stability phenomenon in forward flight is characterized by periodic differential equations. The linearized eigenvalue analysis can be used to determine the system stability. First, linear differential equations are derived for the perturbed motion of the rotorcraft system about the trimmed state. The system eigenvalues are then computed by applying Floquet theory. The eigenvalues that define the system stability of the kth mode are

$$\lambda_k = \alpha_k \pm i\omega_k \tag{3}$$

The kth mode is unstable if $\alpha_k > 0$, and the percent damping of the kth mode is

$$(\%\ \text{damping})_{k\text{th mode}} = -\alpha_k/\omega_k \tag{4}$$

Further details of the analysis are available in Ref. 28.

RS Modeling

RS modeling techniques have been used in the past few years to solve complex, computationally intensive engineering problems.[29] Design of experiments (DOE) theory provides a systematic means of selecting the set of points in the k-dimensional design space at which to perform computational analyses. When the RS techniques are used, the analysis codes are separated from the optimization codes. The complex analysis codes are replaced by the simple polynomials. Second-order or quadratic polynomials are mostly used. A quadratic RS model in k variables of the form

$$y = \beta_0 + \sum_{i=1}^{k} \beta_i x_i + \sum_{i=1}^{k} \sum_{j=1}^{i} \beta_{ij} x_i x_j \tag{5}$$

is used in this paper. The second-order model described in Eq. (5) is a widely used model to describe experimental data in which system curvature is present. Equation (5) contains $1 + 2k + k(k-1)/2$ parameters. As a result, the experimental design used must contain at least $1 + 2k + k(k-1)/2$ distinct design points. In addition, the design must involve at least three levels of each design variable to estimate the pure quadratic terms. There are families of designs available for fitting the second-order model. The central composite designs (CCDs) is one of the popular classes of second-order designs. It involves the use of a two-level factorial or fraction combined with the $2k$ axial or star points. As a result, the design involves 2^k factorial points, $2k$ axial points, and n_c center runs. The factorial points represent a variance optimal design for a first-order model or a first-order plus two-factor interaction type model. Center runs provide information about the existence of curvature in the system. If curvature is found in the system, the addition of axial points allow for efficient estimation of the pure quadratic terms. The choice of α, the axial distance, depends to a great extent on the region of operability and region of interest. The values of axial distance vary from 1.0 to $\sqrt{k}$. For the $k = 2$ case the value of α, the axial distance is $\sqrt{2}$. Figure 1 shows the CCD for $k = 2$. In this case, for $k = 2$, there are four (2^k) factorial points, four ($2 \times k$) axial points, and one center point, resulting in nine points. Also note that for $k = 2$, there are $1 + 2k + k(k-1)/2 = 6$ regression coefficients that need to be determined to find the second-order RS as shown in Eq. (5). The CCD design, therefore, overfits the points to obtain the RS. Therefore, it is able to reduce the error present in any one of the points and avoid the local minima that are not robust and have high sensitivity to change in the design variables.

A quadratic RS for a two-design-variable case has the form

$$y = \beta_0 + \beta_1 x_1 + \beta_2 x_2 + \beta_3 x_1 x_2 + \beta_4 x_1^2 + \beta_5 x_2^2 \tag{6}$$

which has six unknown coefficients, $\beta_0, \beta_1, \ldots, \beta_5$. The $x_1$and x_2 are coded design variables used in the DOE and can be converted to physical design variables using a linear transformation. Let us say, for example, the coded design variable x_1 corresponds to a physical design variable mass per unit length of the rotor blade and x_2 corresponds to the torsional stiffness of the rotor blade. The levels $+1$ and -1 of the coded variable x_1 in Fig. 1 can correspond to 5% increase and decrease from the baseline value of the mass per unit length of the rotor blade, respectively. The baseline value of the blade mass per unit length corresponds to the center point in the x_1 direction. Similarly for the coded variable x_2, $+1$ and -1 can correspond to 25% increase and decrease from the baseline value of the torsional stiffness of the rotor blade. Therefore, once the baseline design at the center point is selected, the factorial points can be defined as percent changes in the baseline, and the axial points are calculated using a linear transformation.

Two major approaches have emerged when integrating RS approximations with nonlinear optimization.[30] The first is the use of global approximations for the entire design space. The second is the use of local approximations, where the RSs are restricted to a region around the current design. The cost of developing a good global RS for a highly nonlinear problem such as helicopter dynamics can be very high. However, within a small neighborhood of the current design point, it can be expected that second-order approximations can be valid, provided the region is properly bounded.

Problem Description

The helicopter rotor optimization problem is divided into two levels, an upper-level optimization and a lower-level optimization. The upper-level optimization is carried out for vibration reduction and aeroelastic stability enhancement. The vibration reduction problem and stability enhancement problem are studied independently. In the upper-level optimization, RS approximations are created for the objective function and constraints. These RS approximations are used for functional evaluations in the optimization process instead of aeroelastic simulations.

Vibration Reduction Problem

The objective function J_v used in this study represents the vibratory hub loads and has been used as a measure of rotorcraft vibration.[3,4] For a four-bladed rotor, the objective function is of the

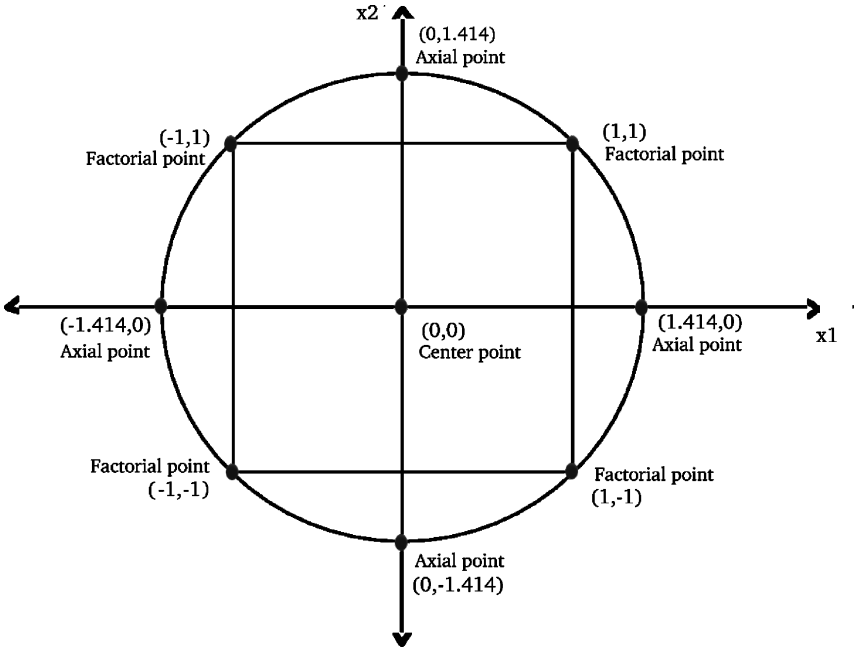

Fig. 1 Central composite design for $k = 2$.

form

$$f(\boldsymbol{X}) = J_v = \sqrt{\left(F_x^{4p}\right)^2 + \left(F_y^{4p}\right)^2 + \left(F_z^{4p}\right)^2} + \sqrt{\left(M_x^{4p}\right)^2 + \left(M_y^{4p}\right)^2 + \left(M_z^{4p}\right)^2} \tag{7}$$

where the forces and moments are nondimensionalized with respect to $m_0\Omega^2R^2$ and $m_0\Omega^2R^3$, respectively.

In the helicopter rotor, the loads observed in the rotating frame are periodic and can be expressed in terms of a Fourier series. The first harmonic of these loads in the rotating frame is generally dominant, and the magnitude of the harmonics declines with the higher harmonics. The 4/revolution hub loads in the fixed frame come from the 3, 4, and 5/revolution loads in the rotating frame. Attempts to minimize the 4/revolution hub loads for a four-bladed hingeless rotor in forward flight can result in an increase in the 1 and 2/revolution blade loads, causing higher dynamic stresses. The lower harmonic blade loads, which are higher in magnitude, are the main sources of dynamic stresses. Therefore, the constraints are imposed on the dynamic stresses caused by the 1 and 2/revolution blade root loads. These constraints avoid reducing the fatigue life of the blade. The constraints are given by

$$J_{d1}^i = \left[\sqrt{\left(F_x^{1p}\right)^2 + \left(F_y^{1p}\right)^2 + \left(F_z^{1p}\right)^2} + \sqrt{\left(M_x^{1p}\right)^2 + \left(M_y^{1p}\right)^2 + \left(M_z^{1p}\right)^2}\right]^i \le J_{d1}^o \tag{8}$$

$$J_{d2}^i = \left[\sqrt{\left(F_x^{2p}\right)^2 + \left(F_y^{2p}\right)^2 + \left(F_z^{2p}\right)^2} + \sqrt{\left(M_x^{2p}\right)^2 + \left(M_y^{2p}\right)^2 + \left(M_z^{2p}\right)^2}\right]^i \le J_{d2}^o \tag{9}$$

where J_{d1}^i and J_{d2}^i are the scalar norm of 1 and 2/revolution blade root loads at the ith iteration of optimization and J_{d1}^o and J_{d2}^o are the baseline values of the same 1 and 2/revolution blade root loads, respectively.

The vibration reduction problem with the constraints can be written in standard notation as minimize

$$J_v = f(\boldsymbol{X}) \tag{10}$$

subject to the constraints

$$g_1(\boldsymbol{X}) = J_{d1}^i - J_{d1}^0 \le 0, \qquad g_2(\boldsymbol{X}) = J_{d2}^i - J_{d2}^0 \le 0 \tag{11}$$

Because the objective function and constraints are approximated with second-order RS models, the optimization problem can be easily solved by a standard gradient-based method.[31] The sequential quadratic programming method is used to solve this constrained optimization problem.

Aeroelastic Stability Enhancement Problem

In this part of study, the objective is to increase the isolated rotor aeroelastic stability in forward flight. Among the three principal motions of the helicopter rotor blade, that is flap, lead–lag, and pitch, the lag mode is usually the least damped. The damping of the lag mode can be increased by changing the cross-sectional properties of the rotor blade. Therefore, the objective function J_s for the rotor aeroelastic stability maximization problem represents the percent damping of the least damped lag mode and is given by

$$J_s = \zeta \tag{12}$$

where ζ is obtained from Floquet theory [Eq. (4)]. The change in the structural properties of the rotor blade for the maximizing of the lag mode damping can result in an increase of vibration level and dynamic stresses. Therefore, constraints are imposed on the vibration level and dynamic stresses acting on the blade. The vibration level and dynamic stresses are constrained to increase by only a percentage c from their baseline values during optimization process.

The stability maximization problem with the vibration and dynamic stress constraints is formulated as maximize

$$J_s = \zeta = f(\boldsymbol{X}) \tag{13}$$

subject to the constraints

$$g_1(\boldsymbol{X}) = J_v - (1+c) * J_v^b \le 0$$
$$g_2(\boldsymbol{X}) = J_{d1} - (1+c) * J_{d1}^b \le 0$$
$$g_3(\boldsymbol{X}) = J_{d2} - (1+c) * J_{d2}^b \le 0 \tag{14}$$

where the J_v, J_{d1}, and J_{d2} are given in Eqs. (7), (8), and (9), respectively. The superscript b denotes their baseline values.

Numerical Results: Upper-Level Problem

For the numerical study, a four-bladed soft-in-plane hingeless rotor blade that is a uniform blade equivalent of the BO105 rotor blade is considered. The rotor properties used in this study are shown in the Table 1. A linear unsteady aerodynamics model is used to predict the airloads.[32] Five spatial finite elements and six time elements are used. For normal mode approximation, four flap modes, four lag modes, and two torsion modes are used. An advance ratio of 0.3, which simulates forward flight condition, is used to obtain the numerical results. The Lock number has to be updated with the change in the values of the blade mass. The Lock number γ is defined as $\gamma = \rho a c_b R^4 / I_b$. Thus, as the blade mass changes, I_b and Lock number also changes.

Vibration Reduction Problem

The cross-sectional properties of the uniform rotor blade are selected as design variables for the optimization problem. The design variables are mass per unit length, flap, lag, and torsional stiffness of the rotor blade. The baseline values of these design variables are given in Table 1. A design space is created around the baseline values of the design variables. From an initial perturbation study, a variation of $\pm 25\%$ from the baseline values of stiffness variables and $\pm 5\%$ from the baseline value of mass design variable are selected to create the design space. As per DOE theory, for the four design variables, $25(2^4 + 2 \times 4 + 1)$ CCD design points are selected within the design space. The aeroelastic analysis is carried out in each of these selected 25 design points. The function values evaluated from the aeroelastic analysis are used to create the RS approximations for the objective function and constraints. Therefore, for the four-design-variables case, only 25 aeroelastic simulations are made to create the RS approximations. The RS approximation created for the objective function J_v is

$$\begin{aligned} J_v = {} & 0.2094 - 0.2498x_1 + 0.1526x_2 - 0.0912x_3 - 0.3304x_4 \\ & - 0.2595(x_1x_2) + 0.1511(x_1x_3) + 0.3460(x_1x_4) \\ & - 0.2440(x_2x_3) - 0.2447(x_2x_4) + 0.1750(x_3x_4) \\ & + 0.0858(x_1)^2 + 0.0766(x_2)^2 + 0.0880(x_3)^2 + 0.0904(x_4)^2 \end{aligned} \tag{15}$$

The RS models created for the dynamic stress constraints are

$$\begin{aligned} J_{d1} = {} & 3.2547 - 0.3910x_1 + 0.8935x_2 - 0.2026x_3 - 0.2714x_4 \\ & - 0.3762(x_1x_2) + 0.1918(x_1x_3) + 0.3481(x_4x_1) \\ & - 0.0985(x_2x_3) - 0.5074(x_2x_4) + 0.3270(x_3x_4) \\ & + 0.0821(x_1)^2 + 0.2508(x_2)^2 + 0.0525(x_3)^2 + 0.0721(x_4)^2 \end{aligned} \tag{16}$$

Table 1 Baseline hingeless blade properties

Property	Value
Number of blades	4
Radius, m	4.94
Hover tip speed, m/s	198.12
m_0, kg/m	6.46
$EI_y/m_0\Omega^2R^4$	0.0108
$EI_z/m_0\Omega^2R^4$	0.0268
$GJ/m_0\Omega^2R^4$	0.00615
m/m_0	1.0
Lock number	5.2
Solidity	0.07
C_T/σ	0.07
c_b/R	0.055

Table 2 Optimum values for vibration reduction

Variable	Reference	At optimum
EI_y	0.0108	0.0062
EI_Z	0.0268	0.0134
GJ	0.00615	0.0033
m	1.0	1.0999

Table 3 Blade frequencies (per revolution) for vibration reduction

Mode	Reference (mode number)	At optimum
Lag bending	0.744 (1)	0.579 (1)
Flap bending	1.146 (2)	1.105 (2)
Flap bending	3.512 (3)	3.097 (3)
Torsion	4.551 (5)	3.223 (4)

$$\begin{aligned} J_{d2} = {} & 0.8693 - 0.0167x_1 + 0.1581x_2 - 0.0769x_3 - 0.1277x_4 \\ & - 0.1759(x_1x_2) + 0.1597(x_1x_3) + 0.2023(x_1x_4) \\ & - 0.1428(x_2x_3) - 0.2319(x_2x_4) + 0.0743(x_3x_4) \\ & + 0.0287(x_1)^2 + 0.0302(x_2)^2 + 0.0218(x_3)^2 + 0.0244(x_4)^2 \end{aligned} \tag{17}$$

Here, the coded variables x_1, x_2, x_3, and x_4 correspond to the physical variables EI_y, EI_z, GJ, and m, respectively. The linear transformation used to convert the coded variables to physical variables is given by $EI_y = (0.0027x_1 + 0.0108)$, $EI_z = (0.0067x_2 + 0.0268)$, $GJ = (0.0015x_3 + 0.00615)$, and $m = (0.05x_4 + 1)$. The RS objective function in Eq. (15) with the constraints in Eqs. (16) and (17) is then minimized. The design variables are constrained to be within the design space defined by the perturbations in the design variables during the optimization process. A reduction of about 15% in the objective function J_v is achieved.

The results from the optimization, using four design variables are presented in Table 2. At the optimum, the frequencies are reduced as shown in the Table 3. The vibration reduction is achieved by destiffening of the blade in flap, lag, and torsion directions and a small increase in blade mass. The frequencies of the lag, flap, and torsion mode are reduced from the baseline values. There is a significant reduction in the blade torsion frequency. Figures 2 and 3 show the 4/revolution hub forces and the 4/revolution hub moments for the baseline and optimal design, respectively. The dominant component of the 4/revolution hub forces in this case is the 4/revolution vertical shear, which is reduced by 23%. Figure 3 shows the 4/revolution hub moments for the baseline and optimal design. The dominant component of the 4/revolution hub moments are the rolling and pitching moments in this case. These are reduced by 23 and 26%, respectively. The relatively smaller yawing moment is also reduced by 50%. The torsional response of the blade for the baseline and the optimum values are shown in Fig. 4. The optimal blade shows a larger nose-down torsional response particularly near the advancing side of the blade, where aerodynamic loads are higher due to high dynamic pressures. The untwisting of the blade results in an alleviation of the higher harmonic loading resulting in lower vibrations.

To check the robustness of the optimal design values, the vibration level at the different advance ratios are evaluated and shown in the Fig. 5. Figure 5 shows that vibration is minimized at different advance ratios, even though the optimization is performed at an advance ratio of 0.3. Also, the rotor modes are found to be stable for the optimal design values. The optimum values shown in Table 2 are checked for robustness to small perturbations. The objective function values in the region around the optimum design point are evaluated using the aeroelastic analysis code. Each variable is given a 3% change from its optimum value while keeping the other variables at their optimums. The objective function values around the optimum also show an average of 15% reduction as given in Table 4. The optimal design obtained is, therefore, robust to small perturbations in the design variables and is, therefore, a practical design.

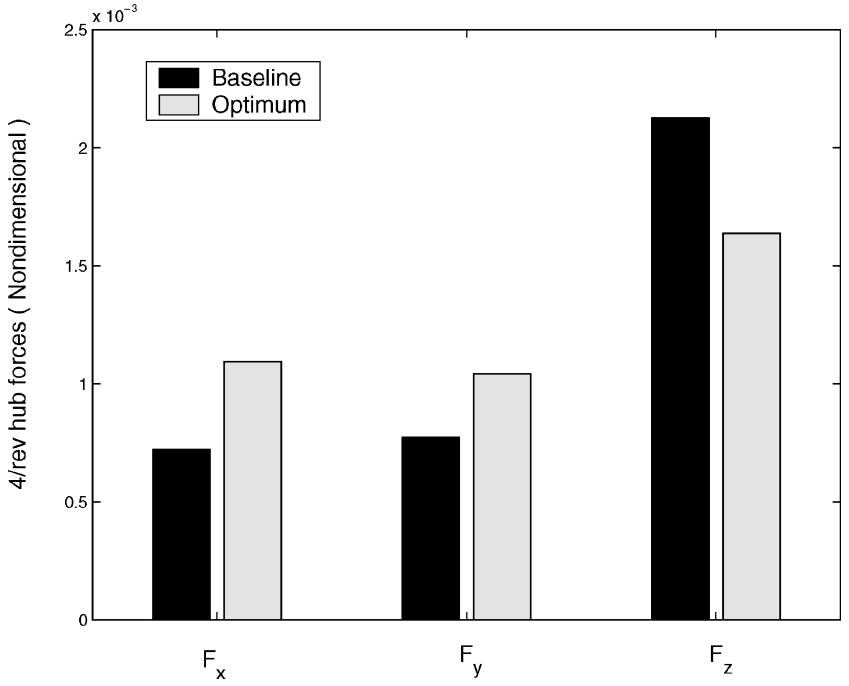

Fig. 2 Vibratory hub loads for vibration reduction problem.

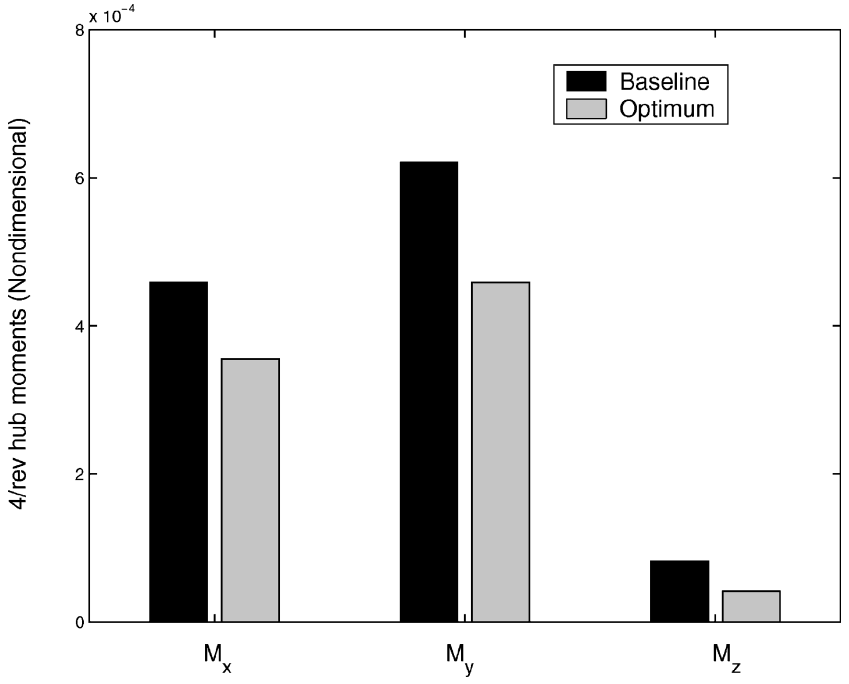

Fig. 3 Vibratory hub moments for vibration reduction problem.

Table 4 Reduction in objective function J_v

Variable	+3%	J_v, %	−3%	J_v, %
EI_y	0.0064	−15.89	0.0060	−10.5
EI_y	0.0138	−14.50	0.0130	−15.3
GJ	0.0034	−15.7	0.0032	−14.8
m	1.132	−18.09	1.066	−13.8

Aeroelastic Stability Enhancement Problem

For the stability enhancement optimization, design variables are mass per unit length, flap, lag, and torsional stiffness of the rotor blade. The rotor properties and flight conditions are the same as for the vibration reduction problem. It is found that the baseline system is stable with the fundamental lag mode being the least damped. The flap and torsion modes are highly damped for the baseline values of the design variables.

Similar to the vibration reduction problem, the aeroelastic stability analyses are carried out at 25 CCD points in the design space for creating RS approximations to the objective function and the constraints. The stability analysis carried out at the CCD points did not show any aeroelastic instability. That is, the least damped mode did not show any instability within the design space. The RS approximation created for the lag mode damping, that is, objective function J_s, is given by

$$\begin{aligned} J_s = {} & 0.61 - 0.0983x_1 + 0.125x_2 - 0.0442x_3 - 0.1858x_4 \\ & - 0.0013(x_1x_2) + 0.0163(x_1x_3) + 0.045(x_1x_4) \\ & - 0.035(x_2x_3) - 0.0337(x_2x_4) + 0.0338(x_3x_4) + 0.0092(x_1)^2 \\ & + 0.0079(x_2)^2 + 0.0117(x_3)^2 - 0.0171(x_4)^2 \end{aligned} \tag{18}$$

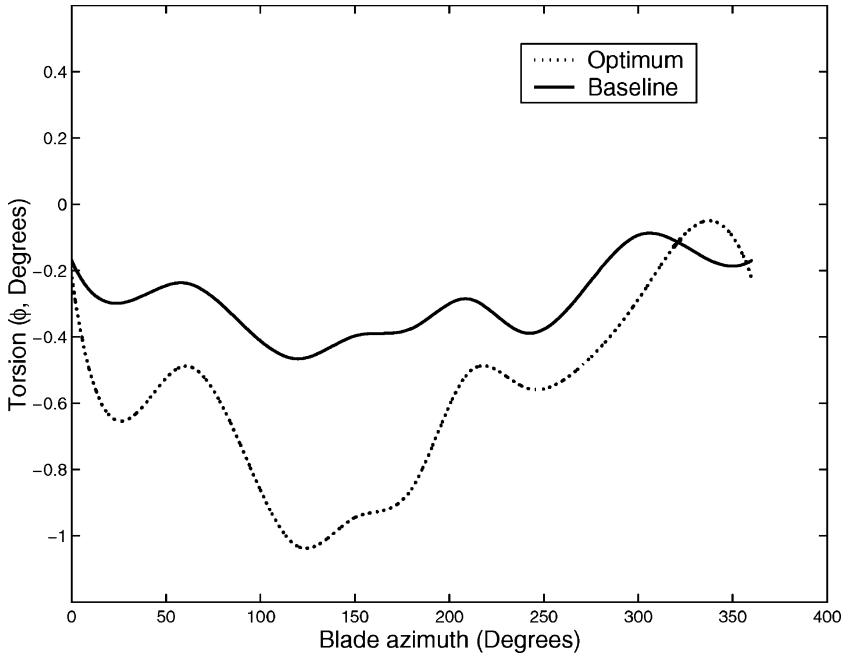

Fig. 4 Blade elastic twist for vibration reduction problem.

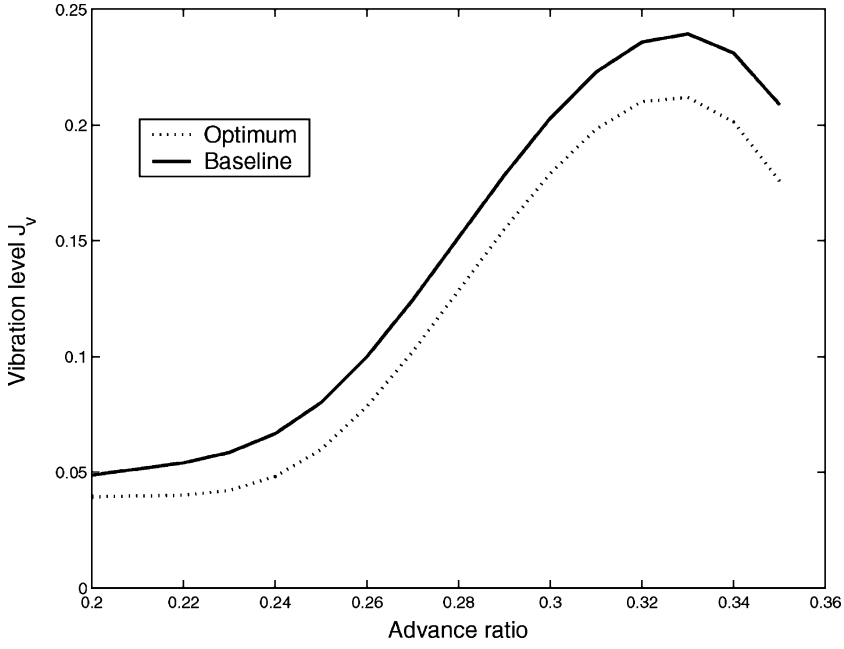

Fig. 5 Vibration objective function at different advance ratios for vibration reduction problem (optimal design at $\mu = 0.3$).

The RS approximation for the vibration level [Eq. (7)] in the same design space is given by

$$\begin{aligned} J_v = {} & 0.0713 - 0.0183x_1 - 0.0173x_2 - 0.0201x_3 - 0.0367x_4 \\ & + 0.0342(x_1x_2) + 0.0359(x_1x_3) + 0.0037(x_1x_4) \\ & + 0.0207(x_2x_3) + 0.0073(x_2x_4) - 0.0104(x_3x_4) \\ & + 0.0027(x_1)^2 + 0.008(x_2)^2 + 0.0122(x_3)^2 + 0.0267(x_4)^2 \end{aligned} \tag{19}$$

For the dynamic stress constraints [Eqs. (8) and (9)],

$$\begin{aligned} J_{d1} = {} & 1.4804 - 0.1749x_1 + 1.0696x_2 + 0.0207x_3 - 1.5929x_4 \\ & - 0.0791(x_1x_2) - 0.0039(x_1x_3) + 0.0907(x_1x_4) \\ & + 0.0420(x_2x_3) - 0.9361(x_2x_4) - 0.0238(x_3x_4) \\ & + 0.0458(x_1)^2 + 0.2243(x_2)^2 + 0.0624(x_3)^2 + 0.7696(x_4)^2 \end{aligned} \tag{20}$$

$$\begin{aligned} J_{d2} = {} & 0.6657 - 0.0568x_1 - 0.0159x_2 + 0.0004x_3 + 0.0031x_4 \\ & + 0.0184(x_1x_2) + 0.0233(x_1x_3) + 0.0096(x_1x_4) \\ & - 0.0018(x_2x_3) + 0.0515(x_2x_4) + 0.0114(x_3x_4) \\ & - 0.0002(x_1)^2 + 0.0048(x_2)^2 - 0.0065(x_3)^2 - 0.0422(x_4)^2 \end{aligned} \tag{21}$$

The stability maximization problem is studied for two cases: unconstrained and constrained. In the unconstrained optimization process, no restrictions are imposed on the dynamic stresses and vibration level while maximizing the damping of the lag mode. In the constrained optimization process, the dynamic stresses and vibration levels are bounded to have only a specified percentage of increase. For the first case, that is, unconstrained optimization, the RS approximation for lag mode damping is employed in the optimization with the upper and lower bounds for each design variable. The upper and

Table 5 Constrained optimization results for stability enhancement

Value of c, %	Increase in damping, %	% Change J_v	Change J_{d1}	Change J_{d2}	Optimal values, $[EI_y, EI_z, GJ, m]$
5	6.56	−15.70	12.32	−7.62	[0.0081 0.0335 0.0051 1.1847]
10	9.84	−15.41	13.79	−7.33	[0.0081 0.0335 0.0050 1.1728]
15	11.48	−14.35	15.27	−7.17	[0.0081 0.0335 0.0049 1.1616]
20	16.39	−13.28	17.21	−7.04	[0.0081 0.0335 0.0048 1.1508]
25	19.67	−12.21	18.91	−6.92	[0.0081 0.0335 0.0047 1.1405]

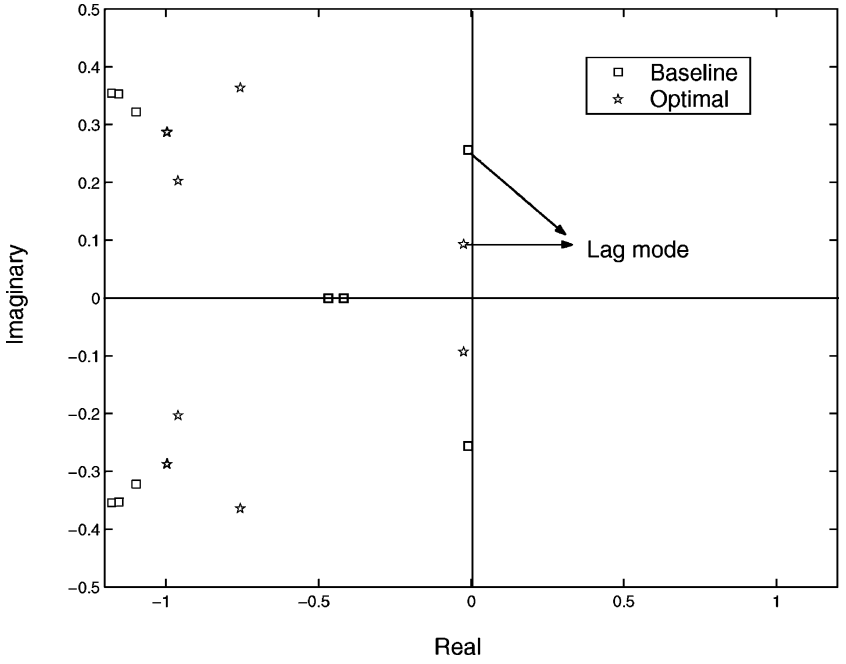

Fig. 6 Stability roots in forward flight for stability enhancement problem; unconstrained optimization.

lower bounds are given as ±25% from the baseline value for each design variable. The damping of the lag mode shows an increase of 125% at the end of the optimization. However, this increase in the damping results in a 59% increase in the vibration level and a 275% increase in the blade root dynamic stresses. At the same time, the stability of the other modes are maintained. The optimal values are $EI_y = 0.0081$, $EI_z = 0.0335$, $GJ = 0.0046$, and $m = 0.75$. The optimal values identified by the RS model are checked with the rotor aeroelastic analysis code. The stability plot for the baseline design and the optimal design is shown in Fig. 6. The least stable roots in the Fig. 6 represent the lag mode stability. Besides the complex-conjugate lag mode eigenvalues, the other modes are well damped.

The unconstrained stability maximization problem resulted in a large increase of vibration and dynamic stresses acting on the blade root. To avoid this, vibration level [Eq. (7)] and dynamic stresses [Eqs. (8) and (9)] are added as constraints in the stability maximization problem. The vibration level and dynamic stresses are allowed to have a specified percentage increase c from their baseline values. The optimization is carried out with these constraints for different values of $c = 5$, 10, 15, and 25%, allowing for different levels of increase in the vibration and dynamic stresses. For $c = 5\%$, the constraints are

$$g_1(X) = J_v - 1.05 \times J_v^b \le 0, \qquad g_2(X) = J_{d1} - 1.05 \times J_{d1}^b \le 0$$

$$g_3(X) = J_{d2} - 1.05 \times J_{d2}^b \le 0 \tag{22}$$

The optimal designs for the different values of c are given in the Table 5. It is clear that efforts to increase aeroelastic stability result in an increase in the 1/revolution dynamic stresses. For stability enhancement, the torsional stiffness and the blade mass appears to be the key design variables, as seen in Table 5, and a reduction in torsion stiffness results in increased stability.

Note that the RS approximations for the objective function and the constraints are created by running aeroelastic analysis code for 25 CCD design points. Then the optimization is carried out to maximize lag damping for different levels of vibration and dynamic stress penalty with the available RS approximations. This shows that, once the RS approximations are created for the objective function and constraints, the designer can find multiple optimal solutions by varying the weighing parameters of the constraints such as c in Eq. (14). In the conventional optimization approach, the whole optimization with aeroelastic simulations has to be repeated for each case. For the results shown in Table 5, only 25 aeroelastic simulations are done, whereas in the conventional optimization procedure six separate optimization processes need to be carried out.

Finally, the optimal design for the unconstrained case is also studied at off-design conditions. Though the optimization is performed at an advance ratio of 0.3, an increase in lag mode damping is also found at other forward speeds, as shown in Fig. 7. As shown in Fig. 8, this increase in the lag mode damping results in a considerable change in blade elastic twist in a manner that is quite different from the vibration reduction results in Fig. 4.

Composite Box-Beam Design: Lower-Level Problem

The upper-level optimization problem ends with the one-dimensional beam optimal stiffness and mass values for the rotor blade. The rotor blade cross section has to be designed with these optimal values. The direct analytical beam formulation proposed by Smith and Chopra[33] is used for predicting the effective elastic stiffness of the composite rotor box beam. They proposed a box-beam design of the cross-sectional properties that were obtained using a

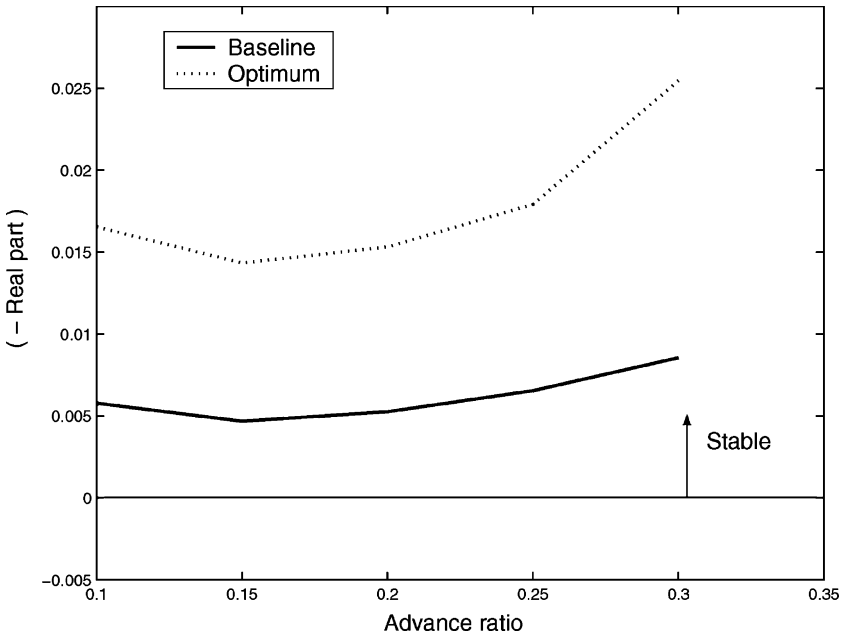

Fig. 7 First lag mode stability at different advance ratios for stability enhancement problem; unconstrained optimization, optimal design at $\mu = 0.3$.

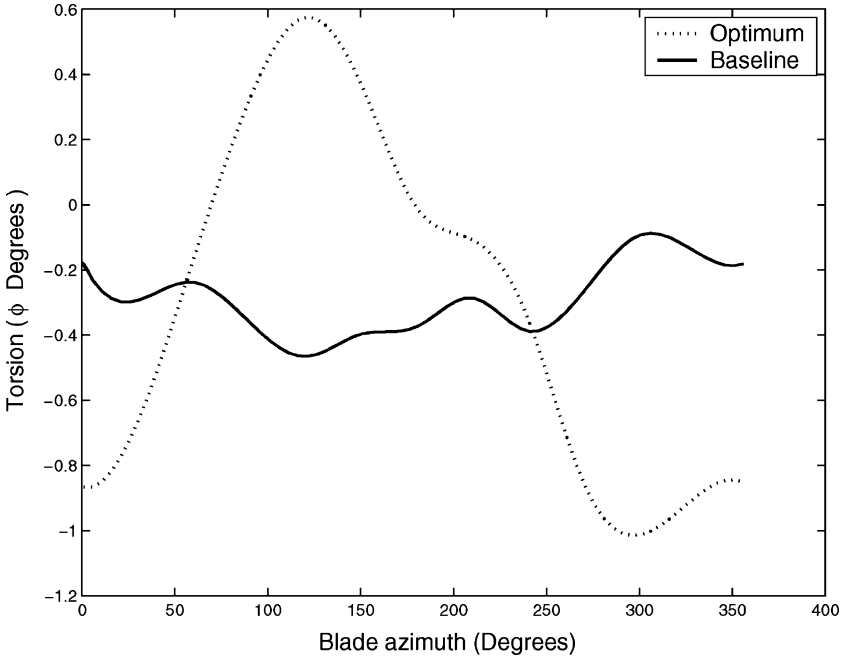

Fig. 8 Blade elastic twist for stability enhancement problem; unconstrained optimization.

manual process to have a reasonable elastic stiffnesses for the rotor blade. The proposed design has outer box-beam dimensions of breadth $b = 4.2$ in. (106.68 mm) and height $h = 2.2$ in. (55.88 mm). Each box-beam wall has 26 plies of thickness 0.005 in. (0.0127 mm). The ply angles were $[0_3/(\pm 15)_3/(\pm 45)_2]_s$. For the detailed modeling of the composite box beam, see Ref. 33. The laminate developed earlier was used in aeroelastic analysis[34] and optimization studies.[3]

For our case, a uniform composite box-beam model is developed for the baseline and optimal solution. The box-beam design proposed in Ref. 33 is taken as the initial guess and is then optimized to have the effective stiffness values near to the baseline and optimal solution of the upper-level problem. The objective function J that is minimized is

$$J = \left(\frac{EI_y^f - EI_y}{EI_y^f}\right)^2 + \left(\frac{EI_z^f - EI_z}{EI_z^f}\right)^2 + \left(\frac{GJ^f - GJ}{GJ^f}\right)^2 \quad (23)$$

where the superscript f represents the final or desired values.

The box-beam breadth b, height h (outer dimensions), and ply angles θ are taken as the design variables with the thickness of the box-beam walls kept constant. The walls are balanced, and the horizontal and vertical walls of the box-beam model are considered to have the same configuration of ply angles. The balanced walls result in no composite couplings, and results in a diagonal stiffness matrix

$$\begin{Bmatrix} Q_x \\ M_x \\ -M_y \\ M_z \end{Bmatrix} = \begin{bmatrix} EA & 0 & 0 & 0 \\ 0 & GJ & 0 & 0 \\ 0 & 0 & EI_y & 0 \\ 0 & 0 & 0 & EI_z \end{bmatrix} \begin{Bmatrix} u_e' \\ \phi' \\ w_b'' \\ v_b'' \end{Bmatrix} \quad (24)$$

For ease of nomenclature, we shall use $EA = k_{11}$, $GJ = k_{22}$, $EI_y = k_{33}$, and $EI_z = k_{44}$ as effective one-dimensional properties of the composite box beam. The wall laminates are symmetric with

26 plies in each wall and are denoted by

$$\theta = [\theta_1, (\pm\theta_2), (\pm\theta_3), (\pm\theta_4), (\pm\theta_5), (\pm\theta_6), (\pm\theta_7)]_s \qquad (25)$$

The ply angle design variables are allowed to take the values as 0, ±45, and ±90 deg during the optimization. The outer layer of the box beam is fixed as $\theta_1 = 0$ deg. These constraints are placed on the design variables to avoid an unrealistic design.

In the preceding optimization problem, the design variables b and h are continuous variables, whereas the ply angles are integer variables. Many optimization studies consider ply angles to be continuous design variables resulting in ply angles such as 10.302, 21.893, and 30.033, which are difficult to manufacture.[24] It is desirable to have discrete ply angles such as 0, ±45, and ±90 deg for manufacturing convenience. The conventional optimization methods to solve such problems requires mixed-integer programming, which is quite complex in nature.[31] However, the preceding optimization problem can be solved without much complexity by using GA. Also, GAs are used here because of their ability to locate near-global solutions. The box beams are designed for the optimal values of the vibration reduction problem and the stability problem, independently.

Low Vibration Blade Cross Section

First, the box-beam design is carried out for the baseline stiffness values given in Table 1 and for optimal stiffness values for the vibration reduction problem given in Table 2. Three composite materials which are graphite/epoxy, boron/epoxy and S-glass/epoxy are selected, and their material properties are given in Table 6. Three box beams are designed for these three materials. The stiffness-to-weight ratios for these composite materials are different. Therefore, upper and lower limits of the design variables breadth and height are selected to be different for the three composite materials. The graphite/epoxy and boron/epoxy have higher stiffness-to-weight ratio compared to S-glass/epoxy. Therefore, the range for box-beam dimensions with the graphite/epoxy and boron/epoxy as composite material are given smaller values. The range for breadth and height is varied between 4–5 in. and 2–3 in. for graphite/epoxy, 3–5 in. and 2–3 in. for boron/epoxy, and 5–7 in. and 3–4 in. for S-glass/epoxy, respectively.

The GA parameters such as crossover rate, mutation rate, and population size are selected to be 0.5, 0.01, and 20, respectively. The objective function J is minimized. The GA is run several times, and the optimum solution is taken as the value that gives the lowest (almost zero) J. The box beams designed for the baseline, and the optimal design values are given in Tables 7 and 8, respectively. The boron/epoxy box beams have the smallest box dimensions, whereas the S-glass/epoxy has the largest box dimensions. This is because the boron/epoxy is much stiffer than the S-glass/epoxy, as shown in Table 6. The graphite/epoxy beams are the lightest due to their low density. The mass of the box beams designed is smaller than the value of the blade mass required to achieve reasonable frequencies given in Table 3. Therefore, nonstructural mass has to be added at the blade quarter-chord to bring it to the level required by the aeroelastic analysis predictions, which is given at the end of Tables 7–10. This addition of mass was also done by Smith and Chopra[33] to arrive at a feasible rotor design.

The use of discrete variables for ply angles, that is, 0, ±45, and 90 deg, actually reduces the computer time needed using GA compared to when continuous design variables are used. Furthermore, the analytical composite box-beam analysis is computationally very fast, thereby permitting the use of GA, which would be very expensive for the upper-level problem. The algorithm in this study is thereby very useful for the performing of preliminary comparative studies in designing box beams with different materials.

Enhanced Stability Blade Cross Section

Composite box beams are also designed for the optimal stiffness values of the aeroelastic stability enhancement problem. The design procedure is the same as that for the box-beam design for the vibration reduction problem. The box beams designed for the optimal values of the unconstrained optimization and the constrained optimization results are given in Tables 9 and 10, respectively. For the constrained optimization results, the box beams are designed for 6.5% increase in damping shown in Table 5, whereas the unconstrained

Table 6 Properties of composite material

Material	E_1, GPa	E_2, GPa	G_{12}, GPa	ν	ρ, kg/m^3
Graphite/epoxy	141.5	9.8	5.9	0.42	1445.4
Boron/epoxy	203.3	18.4	5.6	0.23	2000
S-glass/epoxy	51.5	11.6	1.7	0.25	2100

Table 7 BO105 baseline box-beam design

Box properties	Graphite/epoxy	Boron/epoxy	S-glass/epoxy
Breadth, in.	4.71	4.21	6.91
Height, in.	2.60	2.35	3.85
θ_1, deg	0	0	0
θ_2, deg	0	0	90
θ_3, deg	90	45	45
θ_4, deg	45	45	0
θ_5, deg	0	45	45
θ_6, deg	45	90	90
θ_7, deg	45	0	90
Box-beam mass, kg/m	1.7103	2.1139	3.6969
Nonstructural mass, kg/m	4.7497	4.3461	2.7631

Table 8 BO105 optimal box-beam design for vibration reduction

Box properties	Graphite/epoxy	Boron/epoxy	S-glass/epoxy
Breadth, in.	4.27	3.31	5.44
Height, in.	2.69	2.00	3.32
θ_1, deg	0	0	0
θ_2, deg	90	0	45
θ_3, deg	90	90	90
θ_4, deg	0	0	90
θ_5, deg	45	45	0
θ_6, deg	90	45	45
θ_7, deg	90	45	90
Box-beam mass, kg/m	1.6232	1.6955	2.9959
Nonstructural mass, kg/m	5.4822	5.4098	4.1095

Table 9 Optimal box-beam design for unconstrained stability

Box properties	Graphite/epoxy	Boron/epoxy	S-glass/epoxy
Breadth, in.	4.95	4.84	6.98
Height, in.	2.09	2.03	3.16
θ_1, deg	0	0	0
θ_2, deg	45	90	0
θ_3, deg	0	0	0
θ_4, deg	45	0	45
θ_5, deg	0	45	45
θ_6, deg	45	45	90
θ_7, deg	0	90	90
Box-beam mass, kg/m	1.6433	2.2152	3.4815
Nonstructural mass, kg/m	3.2017	2.6298	1.3635

Table 10 Optimal box-beam design for constrained stability

Box properties	Graphite/epoxy	Boron/epoxy	S-glass/epoxy
Breadth, in.	4.96	4.66	6.9
Height, in.	2.15	2.00	3.01
θ_1, deg	0	0	0
θ_2, deg	45	45	45
θ_3, deg	0	45	0
θ_4, deg	0	0	45
θ_5, deg	45	45	0
θ_6, deg	0	0	0
θ_7, deg	45	90	45
Box-beam mass, kg/m	1.6607	2.1467	3.4016
Nonstructural mass, kg/m	5.9925	5.5064	4.2516

result showed damping increase of about 125%. The comparison of the box-beam results for the stability problem show that the boron-epoxy box beams have the smallest box dimensions, whereas the graphite/epoxy box beams have the lowest weight.

The advantage of the two-level formulation of the optimization can be observed. The composite box-beam optimization is performed using the optimal stiffness values of the upper problem and is independent of the rotor aeroelastic analysis. In conventional single-level optimization, the change in design variables of the box-beam dimension will need a rerun of the aeroelastic analysis, resulting in an increase of computational cost and time. Finally, note that the numerical results in any rotor optimization study are dependent on the configuration and the aeroelastic analysis code used. However, the procedures for optimization developed in this study based on RS approximations for the upper level aeroelastic problem and a GA-based design approach for the box-beam design is applicable for other aeroelastic simulations and composite cross-section design codes.[35,36]

There are several limitations in this study, which will be addressed in future work. Free wake analysis, which is important for vibration prediction, needs to be used.[37] Airfoil cross sections should be considered in place of box-beam models of the blade. Larger vibration reduction and stability enhancement can be obtained by using a nonuniform blade and tailoring the cross section for beneficial composite couplings. Finally, vibration reduction, aeroelastic stability enhancement, and dynamic stress constraints need to be combined using multi-objective optimization.

Conclusions

A four-bladed helicopter rotor optimization problem for vibration reduction and isolated rotor aeroelastic stability enhancement is solved using a two-level approach. At the upper level, the aeroelastic analysis is approximated by polynomial RSs, which are then used to perform optimization. The vibration reduction problem and stability enhancement problem are studied independently. The objective of the vibration reduction problem is to minimize the 4/revolution hub loads with constraints on blade root dynamic stresses. For the aeroelastic stability enhancement problem, the objective is to maximize the damping of the least damped lag mode. Constraints are imposed on the vibration level and dynamic stresses while maximizing the lag mode damping. At the lower level, composite box beams are designed to match the blade optimal stiffnesses of the upper level using GAs. The following conclusions are drawn from this study:

1) Second-order RS approximations based on the central composite design are effective for rotor aeroelastic optimization provided the design variables are restricted to a region of validity. The RS approximations to the aeroelastic analysis in the upper-level problem decouples the analysis problem and the optimization problem because the helicopter aeroelastic analysis is replaced by polynomial function approximations.

2) When the blade flap, lag and torsion stiffness, and blade mass are used as design variables, it is found that vibration reduction of about 15% is obtained using just one RS approximation. The dominant dynamic loads, which are the vertical hub shear and rolling and pitching moments, show reduction of 23, 22.5, and 26%, respectively. The final design is softer in flap, lag, and torsion and shows a small increase in the mass. The vibration reduction is largely due to an elastic untwisting of the blade on the advancing side of the rotor. The optimal design is robust to small perturbations in the design variables. Furthermore, though the optimization is performed at an advance ratio of 0.3, the vibration is reduced at other advance ratios also.

3) For the aeroelastic stability maximization, the lag mode damping is increased by 125% from the baseline provided the constraints are not imposed on hub loads and blade root loads. The constrained optimization results show an increase of 6–20% in the first lag mode damping. However, the increase in stability leads to an increase in the 1/revolution loads acting on the blade root by up to 18%. The lag mode damping is increased with a reduction in the torsional stiffness and an increase in the blade mass from the baseline design. Again, though the optimization is performed at an advance ratio of 0.3, the lag mode damping is also enhanced at other advance ratios.

4) Rotor aeroelastic optimization typically use one-dimensional beam stiffnesses as cross-section design variables. The inverse problem of designing a box beam corresponding to these section properties is addressed using GA. Results show that the GA can be used to obtain ply layups with discrete design values such as 0, ±45, and 90 deg and also to change the dimensions of the box structure. Three different composite materials are used for the box-beam design. It is found that boron/epoxy gives the most compact box-beam design due to its high stiffness properties, whereas graphite/epoxy gives the lowest weight designs due to its lower density. The inverse method of designing allows the possibilities of using different composite materials, which results in the wide range of optimal box-beam configurations for the rotor beam.

References

[1]Friedmann, P. P., and Hodges, D. H., "Rotary Wing Aeroelasticity—A Historical Perspective," *Journal of Aircraft*, Vol. 40, No. 6, 2003, pp. 1019–1046.

[2]Chopra, I., "Review of State of Art of Smart Structures and Integrated Systems," *AIAA Journal*, Vol. 40, No. 11, 2002, pp. 2145–2187.

[3]Ganguli, R., and Chopra, I., "Aeroelastic Optimization of Helicopter Rotor with Composite Coupling," *Journal of Aircraft*, Vol. 32, No. 6, 1996, pp. 1326–1334.

[4]Yuan, K. A., and Friedmann, P. P., "Structural Optimization for Vibratory Loads Reduction of Composite Helicopter Rotor Blades with Advanced Geometry Tips," *Journal of the American Helicopter Society*, Vol. 43, No. 3, 1998, pp. 246–256.

[5]McCarthy, T. R., and Chattopadhyay, A., "A Coupled Rotor/Wing Optimization Procedure for High Speed Tilt Rotor Aircraft," *Journal of the American Helicopter Society*, Vol. 41, No. 4, 1996, pp. 360–369.

[6]Heverly, D., Smith, E. C., and Wang, K. W., "An Optimal Actuator Placement Methodology for Active Control of Helicopter Airframe Vibrations," *Journal of American Helicopter Society*, Vol. 46, No. 4, 2001, pp. 251–261.

[7]Kim, J. E., and Sarigul-Klijn, N., "Elastic-Dynamic Rotor Blade Design with Multiobjective Optimization," *AIAA Journal*, Vol. 39, No. 9, 2001, pp. 1652–1661.

[8]Soykasap, O., and Hodges, D. H., "Performance Enhancement of a Composite Tilt-Rotor Using Aeroelastic Tailoring," *Journal of Aircraft*, Vol. 37, No. 5, 2000, pp. 850–858.

[9]Hathaway, E., and Gandhi, F., "Concurrently Optimized Aeroelastic Couplings and Rotor Stiffness for Alleviation of Helicopter Aeromechanical Instability," *Journal of Aircraft*, Vol. 38, No. 1, 2001, pp. 69–80.

[10]Celi, R., "Optimization-Based Inverse Simulation of a Helicopter Slalom Maneuver," *Journal of Guidance, Control, and Dynamics*, Vol. 23, No. 2, 2000, pp. 289–297.

[11]Spence, A. M., and Celi, R., "Efficient Sensitivity Analysis for Rotary-Wing Aeromechanical Problems," *AIAA Journal*, Vol. 32, No. 12, 1994, pp. 2337–2344.

[12]Ganguli, R., "A Survey of Recent Developments in Rotorcraft Design Optimization," *Journal of Aircraft*, Vol. 41, No. 3, 2004, pp. 493–510.

[13]Fusato, D., and Celi, R., "Multidisciplinary Design Optimization for Aeromechanics and Handling Qualities," *Proceedings of the 28th European Rotorcraft Forum*, No. 2, Sept. 2002.

[14]Lu, Y., and Murthy, V. R., "Sensitivity Analysis of Discrete Periodic Systems with Applications to Helicopter Rotor Dynamics," *AIAA Journal*, Vol. 30, No. 8, 1992, pp. 1962–1969.

[15]Lim, J. W., and Chopra, I., "Aeroelastic Optimization of a Helicopter Rotor Using an Efficient Sensitivity Analysis," *Journal of Aircraft*, Vol. 28, No. 1, 1991, pp. 29–37.

[16]Ganguli, R., and Chopra, I., "Aeroelastic Optimization of Helicopter Rotor to Reduce Vibration and Dynamic Stresses," *Journal of Aircraft*, Vol. 12, No. 4, 1996, pp. 808–815.

[17]Patrick, N. K., "Statistical Approximations for Multidisciplinary Design Optimization: The Problem of Size," *Journal of Aircraft*, Vol. 36, No. 1, 1999, pp. 275–286.

[18]Venter, G., Haftka, R. T., and Starnes, J. H., Jr., "Construction of Response Surface Approximations for Design Optimization," *AIAA Journal*, Vol. 36, No. 12, 1998, pp. 2242–2249.

[19]Hosder, S., Watson, L. T., Grossman, B., Mason, W. H., Kim, H., Haftka, R. T., and Con, S. E., "Polynomial Response Surface Approximations for the Multidisciplinary Design Optimization of a High Speed Civil Transport," *Optimization and Engineering*, Vol. 2, No. 4, 2001, pp. 431–452.

[20]Henderson, J. L., Walsh, J. L., and Young, K. C., "Application of Response Surface Techniques to Helicopter Rotor Blade Optimization Procedure," *Proceedings of the AHS National Technical Specialist Meeting*

on Rotorcraft Structures: Design Challenges and Innovative Solutions, American Helicopter Society, Alexandria, VA, 1995.

[21]Lee, J., and Hajela, P., "Parallel Genetic Algorithm Implementation in Multidisciplinary Rotor Blade Design," *Journal of Aircraft*, Vol. 33, No. 5, 1996, pp. 962–969.

[22]Ganguli, R., "Optimum Design of Helicopter Rotor for Low Vibration using Aeroelastic Analysis and Response Surface Methods," *Journal of Sound and Vibration*, Vol. 258, No. 2, 2002, pp. 327–344.

[23]Soykasap, O., "Inverse Method in Tilt-Rotor Optimization," *Aerospace Science and Technology*, Vol. 5, No. 7, 2001, pp. 437–444.

[24]Paik, J., Volovoi, V. V., and Hodges, D. H., "Cross-Sectional Sizing and Optimization of Composite Blades," AIAA Paper 2002-1322, April 2002.

[25]Adams, D. B., Watson, L. T., and Gurdal, Z., "Optimization and Blending of Composite Laminates Using Genetic Algorithms with Migration," *Mechanics of Composite Materials and Structures*, Vol. 10, No. 3, 2003, pp. 183–203.

[26]Goldberg, D., *Genetic Algorithms in Search, Optimization, and Machine Learning*, Pearson Education, 2001.

[27]Hodges, D. H., and Dowell, E. H., "Nonlinear Equations of Motion for the Elastic Bending and Torsion of Twisted Nonuniform Blades," NASA TND-7818, Dec. 1974.

[28]Bir, G., et al., "University of Maryland Advanced Rotorcraft Code (UMARC) Theory Manual," UM-AERO Rept., 92-02, Dept. of Aerospace Engineering, Univ. of Maryland, College Park, MD, 1992.

[29]Myers, R. H., and Montgomery, D. C., *Response Surface Methodology: Process and Product Optimization using Designed Experiments*, Wiley, 1995, New York.

[30]Perez, V. M., Renaud, J. E., and Watson, L. T., "Adaptive Experimental Design for Construction of Response Surface Approximations," *AIAA Journal*, Vol. 40, No. 12, 2000, pp. 2495–2503.

[31]Belegundu, A. D., and Chandrupatla, T. R., *Optimization Concepts and Applications in Engineering*, Prentice Hall, Upper Saddle River, New Jersey, 1999.

[32]Leishman, J. G., and Beddoes, T. S., "A Generalized Model for Unsteady Aerodynamic Behavior and Dynamic Stall using the Indicial Method," *Journal of the American Helicopter Society*, Vol. 36, No. 1, 1990, pp. 14–24.

[33]Smith, E. C., and Chopra, I., "Formulation and Evaluation of an Analytical Model for Composite Box-Beams," *Journal of American Helicopter Society*, Vol. 36, No. 3, 1991, pp. 23–35.

[34]Smith, E. C., and Chopra, I., "Aeroelastic Response, Loads, and Stability of a Composite Rotor in Forward Flight," *AIAA Journal*, Vol. 31, No. 7, 1993, pp. 1265–1273.

[35]Volovoi, V. V., Hodges, D. H., Cesnik, C. E. S., and Popescu, B., "Assessment of Beam Modeling Methods for Rotor Blade Applications," *Mathematical and Computer Modelling*, Vol. 33, No. 10-11, 2001, pp. 1099–1112.

[36]Jung, S. N., Nagaraj, V. T., and Chopra, I., "Assessment of Composite Rotor Blade Modeling Techniques," *Journal of the American Helicopter Society*, Vol. 44, No. 3, 1999, pp. 188–205.

[37]Datta, A., and Chopra, I., "Validation of Structural and Aerodynamic Modeling Using UH-60A Flight Test Data," *Proceedings of the American Helicopter Society 59th Annual Forum*, American Helicopter Society, Alexandria, VA, May 2003, pp. 1028–1042.